Article

A Low Frequency Noise Source Localization and Identification Method Based on a Virtual Open Spherical Vector Microphone Array

Boquan Yang [1], Yuan Gao [1], Qiang Guo [1] and Shengguo Shi [1,2,3,*]

1 College of Underwater Acoustic Engineering, Harbin Engineering University, Harbin 150001, China
2 Key Laboratory of Marine Information Acquisition and Security, Harbin Engineering University, Ministry of Industry and Information Technology, Harbin 150001, China
3 National Key Laboratory of Underwater Acoustic Technology, Harbin Engineering University, Harbin 150001, China
* Correspondence: shishengguo@hrbeu.edu.cn

Abstract: Aiming at the problem of poor spatial resolution of low-frequency noise sources in a small-aperture spherical microphone array (SMA), this paper proposes a method for localizing and identifying low-frequency noise sources based on virtual-vector open SMA ('p+v' joint processing method of pressure and velocity). Firstly, a virtual open SMA with a larger aperture is obtained using a virtual array extrapolation method. In this method, the virtual SMA and the actual SMA are regarded as a dual-radius SMA, and velocity information is obtained using finite difference elements of the same direction (azimuth and elevation) array of the virtual and actual SMA. At the same time, the sound pressure at the velocity position is obtained using the virtual SMA extrapolation method and the virtual vector array element SMA, whereby both velocity and sound pressure information is obtained. Finally, the vector signal processing technology is introduced into the generalized inverse beamforming algorithm (GIB). After determining the vector transfer function of the 'p+v' joint processing mode, a low-frequency-noise-source localization and identification method based on the vector signal processing GIB is proposed. The simulation and experiment results show that a virtual SMA with a large aperture can be obtained using a virtual array extrapolation method, and the GIB with sound pressure and velocity joint processing has a better spatial resolution.

Keywords: low frequency noise source; vector signal processing; spherical array; virtual spherical array extrapolation; generalized inverse beamforming

1. Introduction

Beamforming technology with spherical microphonge arrays (SMAs) is widely used in localizing and identifying noise sources in the mid–high-frequency range because of its small size, full space directivity, and good resolution in medium and high frequencies [1–3]. In recent years, low-frequency noise sources have attracted extensive research attention. Therefore, it is essential to develop a low-frequency-noise-source localization and identification method using a small-aperture SMA.

An SMA, used in combination with the spherical harmonic beamforming (SHB) algorithm, is the most commonly used noise-source localization and identification method in the mid–high-frequency range. This method decomposes the sound field into a superposition of spherical harmonic functions and achieves the localization and identification of noise sources through the orthogonality of the spherical harmonic functions [1,4]. However, it is necessary for the SHB algorithm to reasonably select the truncation order of the spherical harmonic function according to the number of SMA elements. Furthermore, the SHB algorithm is vulnerable to noise and sidelobe interference in the application process, which leads to a poor localization effect [3,4]. In addition, the small aperture of the SMA limits the

frequency range of the SHB algorithm's application, especially due to its poor localization effect of low-frequency noise sources [5,6].

In order to more accurately localize noise sources, scholars have provided solutions in two aspects, based on extensive research. On the one hand, scholars have improved the beamforming effect using algorithms. Hald proposed a filter and sum (FAS) beamforming algorithm to effectively suppress the side lobes of the beam [7]. Scholars have improved the spatial resolution of sound source localization by using clear algorithms for sound source identification, such as DAMAS, CLEAN, etc. [8]. On the other hand, researchers have improved the applicable frequency range by redesigning the physical structure of a spherical array. B. Rafaely discussed the design method of an SMA and provided an optimal layout scheme of microphones [9]. I. Balmages and B. Rafaely et al. designed a double-layer open SMA to overcome the instability of the single-layer open SMA at the nadal of the spherical Bessel functions, as well as broadening the applicable frequency range of a single-layer open SMA [10,11]. C. T. Jin put forward another design and optimization method of double-layer SMA that arranged an open sphere at a certain distance outside the rigid SMA. Furthermore, the author discussed the advantages of this SMA in improving the frequency range and the optimal design of the SMA [12]. Using different traditional methods, in this paper, we consider both algorithms and the extrapolated aperture technique to achieve a better localization performance for the localization of low-frequency noise sources, which does not affect the aperture and the element number of the actual SMA.

In this paper, a virtual SMA with a large aperture is first obtained by extrapolating the SMA, and its ability to localize low frequencies is verified by generalized inverse beamforming algorithm (GIB) [5]. Then, the virtual SMA and actual SMA are combined to form a virtual double-layer open SMA, and a virtual SMA with velocity elements is obtained by the finite difference for all the same azimuth elements. In addition, because vector signal processing technology can improve the effect of low-frequency applications by simultaneously using sound pressure and velocity, this paper presents the transfer function of 'sound pressur–velocity' and proposes the joint processing method of sound pressure and velocity of the obtained virtual vector SMA. The proposed method can effectively improve the low-frequency localization performance of the actual SMA.

The remainder of this paper is arranged as follows: Section 2 gives the theory of the virtual SMA extrapolation method. In Section 3, an SMA noise source localization method based on GIB is briefly described. And the GIB of the joint processing method of sound pressure and velocity is proposed. Section 4 gives the simulation experiments of low-frequency noise source localization and identification with GIB. Section 5 is devoted to verifying the accuracy of simulation conclusions and the effectiveness of practical applications through noise source localization and identification experiments. The conclusions are provided in Section 6.

2. Virtual SMA Extrapolation Method

Based on the inverse problem theory of sound field reconstruction, it is assumed that there is a spherical envelope outside the SMA (with the same spherical center as the SMA), there are several virtual sources on the envelope surface, and the data received by the SMA element is assumed to be the result of the radiation superposition of the virtual sound sources on the envelope surface. The extrapolation of the virtual SMA is realized through the optimal solution of the virtual source strength on the envelope surface and the sound field transmission relationship between the virtual source and any point in the envelope surface [13–15]. The extrapolation diagram of spherical array is shown in Figure 1.
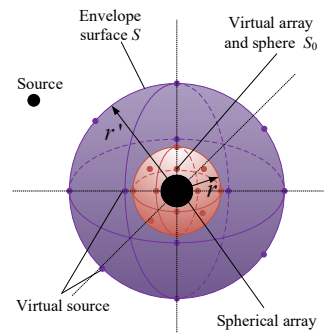
Figure 1. Schematic diagram of virtual spherical array extrapolation.

Assuming that there is a virtual source on the envelope surface S radiating from the external actual sound source to the envelope surface, the sound pressure p of the virtual sound source at S at any point r satisfies the improved Helmholtz equation [5]:

$$\nabla^2 p_{r'}(r) + k^2 p_{r'}(r) = \delta(r - r') \tag{1}$$

where k is wavenumber, and $k = \omega/c$, ω represents angular frequency, c is sound speed in the air.

Then it can be obtained that the sound field of the virtual source on the envelope S and inside S is

$$p(r) = \int_{\partial\Delta} G(r,r')q(r')dS(r') \tag{2}$$

where $q(r')$ is virtual sources strengths, $G(r,r')$ is the free field Green function, $p(r)$ is the sound pressure.

In the actual calculation, it is assumed that M virtual sources are uniformly distributed on the envelope surface S, and the integral formula in Equation (2) is discretized and written in matrix form:

$$\mathbf{p}(\mathbf{r}_l) = \mathbf{G}(\mathbf{r}_l, \mathbf{r}'_m)\mathbf{q}(\mathbf{r}'_m) \tag{3}$$

where $\mathbf{p}(\mathbf{r}_l)$ represents the received signal vector of the spherical array element, and $\mathbf{G}(\mathbf{r}_l, \mathbf{r}'_m)$ represents the transfer function between the virtual source and the SMA element. The source strength of the virtual source can be obtained by inverting the above equation:

$$\mathbf{q} = \mathbf{G}^{-1}\mathbf{p} \tag{4}$$

In the actual inversion calculation process, usually, the number of array elements does not match the number of virtual sources on the envelope surface. $\mathbf{G}$ is a non-square matrix, and the direct inversion result is unstable. The result will have a serious deviation from the real value. A regularization method is needed to obtain a stable solution of the above equation in the solution process. Tikhonov regularization is based on the idea of minimizing the joint weighting between the residual parametrization and the solution parametrization of the above equation, i.e.,

$$\mathbf{q}_{reg} = \arg\min\left\{\|\mathbf{p} - \mathbf{Gq}\|_2^2 + \lambda^2\Omega(\mathbf{q})^2\right\} \tag{5}$$

where $\Omega(\mathbf{q}) = \|\mathbf{Lq}\|^2$ is the discrete smoothing norm, which constrains the smoothness of the undetermined solution. $\mathbf{L}$ is the penalty matrix, when $\mathbf{L}$ is the unit matrix, this method is called the standard Tikhonov regularization method, and λ is the regularization parameter. In general, the traditional regularization methods tend to produce an overly smooth solution. However, in practice, the solution is likely to have the property of discontinuity or sharp corners and other unsmooth properties, which will lead to the loss of part of the information, and thus the accurate regularization solution cannot be obtained. To overcome the shortcomings of traditional regularization and obtain a stable solution,

the accuracy of the regularization solution can be improved by modifying the regularization matrix in the Tikhonov regularization process, and the regularization matrix is defined, which is also called the beamforming regularization matrix $\mathbf{L} = \text{diag}(|\mathbf{G}^H\mathbf{p}|/||\mathbf{G}^H\mathbf{p}||_\infty)^{-1}$. Therefore, the solution of source strength on the envelope surface can be written as [14,15]:

$$\mathbf{q}_{BF} = \frac{\mathbf{G}^H\mathbf{p}}{\mathbf{G}^H\mathbf{G} + \lambda^2\mathbf{L}^H\mathbf{L}} \tag{6}$$

Based on the above theoretical analysis, if the virtual source strength $\mathbf{q}_{BF}$ on the envelope surface S can be obtained, the sound pressure value of any field point inside the envelope surface can be approximately calculated, that is, the approximate sound pressure data on any spherical surface inside S can be obtained without changing the array aperture, thus realizing the SMA extrapolation.

3. Noise Source Localization Method Using GIB with 'p+v' Joint Processing

In order to further improve the resolution of a virtual extrapolated array (EA) for the localization of sound sources in the low frequency range, a GIB beamforming algorithm is adopted in this paper. Considering the advantage of a vector microphone in the low frequency range, a GIB based on 'p+v' joint processing is proposed.

3.1. Noise Source Localization and Identification Method with GIB

GIB estimates the sound source information through the data measured by the array and its sound field transfer relationship (Equation (4)). Generally, the number of microphones used is less than the number of grid points scanned on the sound source surface, so the solution of the source intensity of the grid points on the sound source surface can be written as:

$$\mathbf{q}_{\lambda\beta} = \left(\mathbf{L}^H\mathbf{L}\right)^{-1}\mathbf{G}^H\left(\mathbf{G}\left(\mathbf{L}^H\mathbf{L}\right)^{-1}\mathbf{G}^H + \lambda^2\mathbf{I}\right)^{-1}\beta\mathbf{p} \tag{7}$$

where β is the scaling parameter used to compensate for the reduced source amplitude caused by over-regularization, and its mathematical expression is $\beta = ||\mathbf{G}\mathbf{L}^{-1}(\mathbf{G}\mathbf{L}^{-1})^H + \lambda\mathbf{I}||_2$, $\mathbf{q}_{\lambda\beta}$ is the result of GIB [13].

3.2. GIB Based on the Joint Processing of 'p+v'

The transfer relationship in the above GIB algorithm is the free-field Green function. However, when using the vector microphones for an SMA, the transmission relationship should consider the transmission relationship of velocity. Therefore, the transfer function derivation process of the GIB method, based on vector microphone and its 'p+v' sound pressure and velocity joint processing, is carried out as follows: The sound pressure and velocity in the steady state sound field can be directly measured through the vector microphone. At the same time, the sound pressure and velocity meet the Euler formula:

$$\nabla p = j\omega\rho v \tag{8}$$

where ∇ represents gradient, j represents imaginary unit and ρ represents air density.

At the same time, the sound pressure at position r_v can be written as follows:

$$p_v = G(s, r_v)Q = \frac{e^{jkr_v}}{4\pi r_v}Q \tag{9}$$

where $G(s, r_v)$ represents the sound field transfer function (free field Green function) from the sound source to the velocity position and Q is the source intensity at the grid point on the sound source surface.

The partial derivative of the sound pressure is calculated at this position, namely:

$$\frac{\partial p_v}{\partial r_v} = \frac{jke^{jkr_v}4\pi r_v - 4\pi e^{jkr_v}}{16\pi^2 r_v^2}Q = \frac{jkr_v - 1}{4\pi r_v^2}e^{jkr_v}Q \tag{10}$$

By introducing the above formula into Euler's formula, we can get the velocity:

$$v = \frac{1}{j\omega\rho}\nabla p = \frac{1}{j\omega\rho}\frac{jkr_v - 1}{4\pi r_v^2}e^{jkr_v}Q = \frac{jkr_v - 1}{j\omega\rho r_v}p_v \tag{11}$$

Divide the numerator and denominator of the above formula by jkr_v at the same time, and the velocity can be simplified as:

$$v = \frac{1 + j\lambda/2\pi r_v}{\rho c}p_v \tag{12}$$

According the 'p+v' joint treatment mode, is adopted, the combination form can be expressed as:

$$p_v + v = \frac{1 + \rho c + j\lambda/2\pi r_v}{\rho c}p_v = \frac{1 + \rho c + j\lambda/2\pi r_v}{4\pi\rho c r_v}e^{jkr_v}Q \tag{13}$$

It can be seen from the above formula that after the joint treatment of 'p+v', the sound field transfer function is equal to:

$$G_{pv} = \frac{1 + \rho c + j\lambda/2\pi r_v}{4\pi\rho c r_v}e^{jkr_v} \tag{14}$$

When there are no vector microphones, the velocity in the sound field cannot be directly measured. An alternative method to measure velocity uses the finite difference of the two sound pressure microphones in the same direction. A schematic diagram of this differential principle is shown in Figure 2.
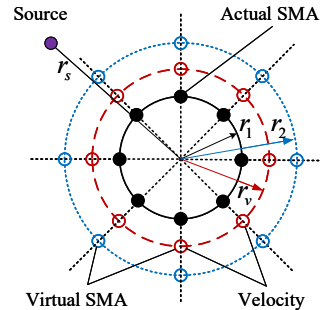

Figure 2. Difference schematic diagram of dual-radius spherical array. The black circle and dot represent the actual SMA and the array element respectively, and the red and blue represent the virtual SMA. In addition, the red circle also indicates the position of the velocity obtained by the difference.

The sound pressure gradient is equal to:

$$\nabla p = \frac{p_1 - p_2}{r_1 - r_2} = \frac{G(s,r_1)Q - G(s,r_2)Q}{r_1 - r_2} = \frac{G(s,r_1) - G(s,r_2)}{r_1 - r_2}Q \tag{15}$$

The velocity can be obtained by substituting the above equation into Equation (8):

$$v = \frac{1}{j\omega\rho}\frac{G(s,r_1) - G(s,r_2)}{r_1 - r_2}Q \tag{16}$$

where, $G(s,r_1) - G(s,r_2)/j\omega\rho(r_1 - r_2)$ is the transfer function from the velocity point to the sound source, and the sound pressure at the velocity point can be approximated as $p_v = (p_1 + p_2)/2$ (The sound pressure at this point can also be obtained according to the virtual SMA extrapolation method).

According to Equations (15) and (16), the combined form of 'p+v' is

$$p_v + v = \left(\frac{G(s,r_1) + G(s,r_2)}{2} + \frac{1}{j\omega\rho} \frac{G(s,r_1) - G(s,r_2)}{r_1 - r_2} \right) Q = G_{pv} Q \qquad (17)$$

It can be seen from the above formula that the sound field transfer function after the joint treatment of 'p+v' is

$$G_{pv} = \frac{G(s,r_1) + G(s,r_2)}{2} + \frac{1}{j\omega\rho} \frac{G(s,r_1) - G(s,r_2)}{r_1 - r_2} \qquad (18)$$

Substitute the transfer function G_{pv} of the sound pressure velocity joint processing method into the GIB algorithm, there can obtain the output results of the GIB based on the 'p+v' joint processing:

$$\mathbf{q}_{\lambda\beta} = \left(\mathbf{L}^H \mathbf{L} \right)^{-1} \mathbf{G}_{pv}^H \left(\mathbf{G}_{pv} \left(\mathbf{L}^H \mathbf{L} \right)^{-1} \mathbf{G}_{pv}^H + \lambda^2 \mathbf{I} \right)^{-1} \beta \mathbf{p} \qquad (19)$$

Because the virtual concentric dual-radius open SMA in this paper is obtained using a virtual SMA extrapolation method, the joint processing transfer function obtained by the finite difference method needs to be substituted into the GIB algorithm to achieve noise source localization and identification.

After measuring velocity by using the dual-radius open SMA element with the same azimuth for differential processing, the sound pressure information of the velocity point location is obtained. In previous studies, the mean value method $((p_1 + p_2)/2)$ was used to obtain the sound pressure. However, in this paper, the virtual SMA extrapolation method can also be used to solve the approximate sound pressure at this point. According to the process of the proposed method, we next provide an error comparison of the two calculation methods.

In this paper, the sound field on a virtual sphere (the sphere is between the actual SMA and the sound source) is reconstructed by the virtual SMA extrapolation method, and M points (virtual SMA elements) are taken out on the sphere (the azimuth and elevation of these points are the same as elements of the actual SMA). In order to evaluate the data accuracy of virtual SMA elements, the normalized least squares reconstruction error ε of these points is [16]:

$$\varepsilon = \frac{\sum\limits_{i}^{M} \left(\| p_{the}(r,\theta_i,\varphi_i) - p_{rec}(r,\theta_i,\varphi_i) \|_2 \right)^2}{\sum\limits_{i}^{Q} \left(\| p_{the}(r,\theta_i,\varphi_i) \|_2 \right)^2} \times 100\% \qquad (20)$$

where p_{the} and p_{rec} are the theoretical and approximate values of sound pressure on the virtual sphere, respectively.

Figure 3 shows the sound pressure at the velocity point calculated by the SMA extrapolation method and mean value method, respectively. Figure 3a shows the sound pressure results and theoretical values calculated by the above two methods, respectively, when the sound source frequency is 500 Hz. Figure 3b shows the calculation error of the two calculation methods when the sound source frequency is 100–1000 Hz. (Simulation conditions: sound source distance is 1 m, simulated spherical array radius is 0.3 m, virtual spherical array radius is 0.4 m, SNR = 20 dB, and sound velocity in air c = 340 m/s.) Figure 3a shows that the two methods can effectively calculate the sound pressure at the velocity point, and the calculation results are accurate with the exception of a few points. Figure 3b shows that the sound pressure error at this point increases with the increase in sound source frequency, causing a decrease in the error values of the results calculated by the virtual array extrapolation method.
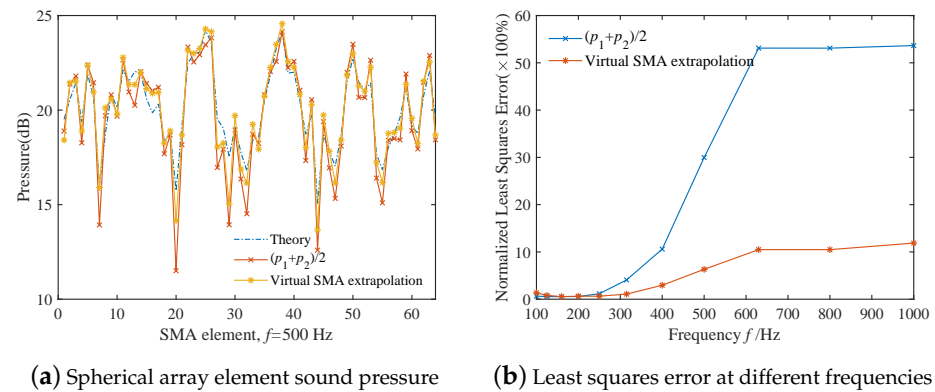
(**a**) Spherical array element sound pressure   (**b**) Least squares error at different frequencies

Figure 3. Calculation and comparative analysis of sound pressure at velocity point.

4. Simulation Calculation of Noise Source Localization and Identification

From the above simulation results of the velocity points, the virtual SMA extrapolation method can accurately calculate the sound pressure at the velocity points. Moreover, the extrapolation method can effectively obtain a virtual array with a larger aperture. In this section, the simulation experiments of single and double sound source localization and identification are carried out to investigate the localization performance and the advantages of the proposed method. Figure 4 shows the schematic diagram of the virtual SMA noise source.
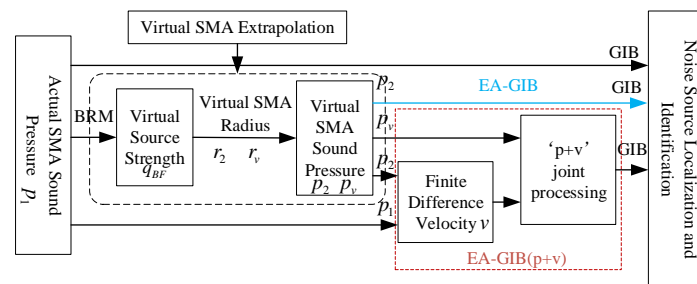

Figure 4. Schematic diagram of the virtual SMA noise source localization and identification.

4.1. Single Sound Source Simulation

In the simulation, an open SMA with 64 elements (randomly and uniformly distributed) with a radius of 0.3 m is taken as the simulation object, which is refer to as the actual SMA. The sound source is placed at a specific point $(1 \text{ m}, 89°, 160°)$ in the spherical coordinate system where the SMA is located (the geometric center of the SMA is the coordinate origin), where SNR = 20 dB. The radius of the virtual SMA with vector elements obtained using the virtual spherical array extrapolation method is set to 0.45 m, and its element direction is same as that of the actual SMA.

Figures 5 and 6 show the simulation localization and identification results of the single sound source with the frequency 125 and 500 Hz, respectively. Figures 5 and 6 show that the GIB with a virtual SMA is significantly more accurate localization ability. In addition, the GIB based on 'p+v' joint processing has a narrower main lobe than other methods. This not only proves the effectiveness of the virtual SMA extrapolation method explored in this paper, but also proves the advantages of the sound pressure and velocity joint processing method in the localization of the low-frequency noise source.
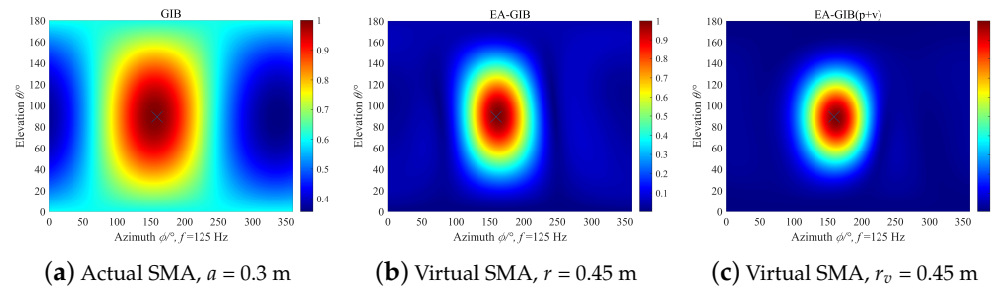
(**a**) Actual SMA, *a* = 0.3 m　　(**b**) Virtual SMA, *r* = 0.45 m　　(**c**) Virtual SMA, r_v = 0.45 m

Figure 5. Simulation results of the single sound source with the frequency 125 Hz.

(**a**) Actual SMA, *a* = 0.3 m　　(**b**) Virtual SMA, *r* = 0.45 m　　(**c**) Virtual SMA, r_v = 0.45 m
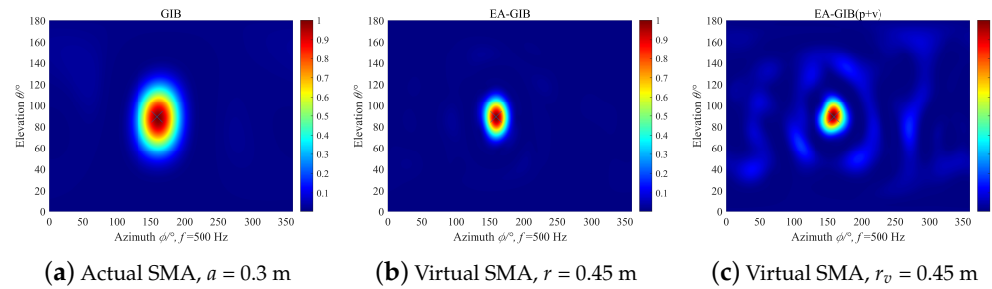
Figure 6. Simulation results of the single sound sources with the frequency 500 Hz.

4.2. Double Sound Source Simulation

The two sound sources are placed at $(1\,\text{m}, 91°, 78°)$ and $(1\,\text{m}, 89°, 160°)$ in the spherical coordinate system, and the other simulation conditions are same as those for for a single-sound-source simulation.

Figures 7 and 8 show the simulation localization and identification results of double sound sources with the sound source frequency 125 and 500 Hz, respectively. Subgraph (a) to (c), as shown in Figures 7 and 8, represent the results of the actual SMA test with a radius of 0.3 m, the virtual SMA with a radius of 0.45 m, and the virtual SMA with a radius of 0.45 m (vector open SMA), respectively. Figure 7 shows that, when the sound-source frequency is equal to 125 Hz, the actual SMA cannot distinguish between two sound sources, while the virtual open SMA with a large aperture can effectively distinguish between two sound sources, proving the effectiveness of the virtual SMA extrapolation method. By comparing Figure 7b,c, it can be found that the resolution effect of the two sound sources is more significant after the joint processing of sound pressure and velocity, proves the effectiveness of the GIB method based on the joint processing of sound pressure and velocity proposed in this paper for localizing low-frequency sound sources.
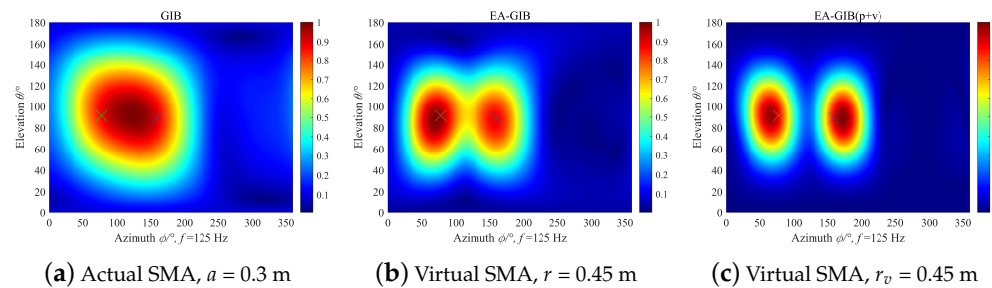

(**a**) Actual SMA, *a* = 0.3 m　　(**b**) Virtual SMA, *r* = 0.45 m　　(**c**) Virtual SMA, r_v = 0.45 m

Figure 7. Simulation results of the double sound source with the frequency 125 Hz.

(**a**) Actual SMA, *a* = 0.3 m (**b**) Virtual SMA, *r* = 0.45 m (**c**) Virtual SMA, r_v = 0.45 m
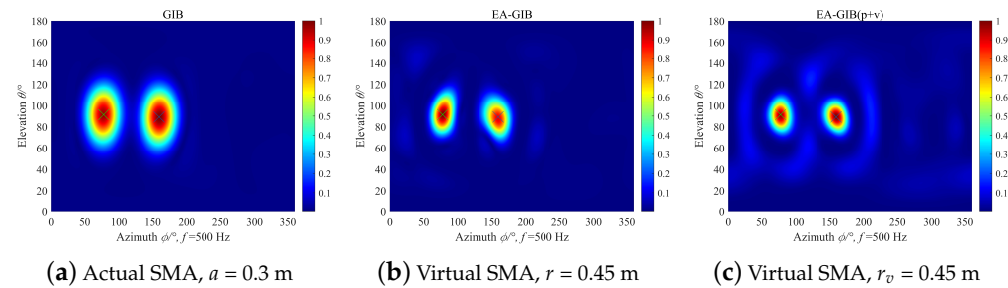
Figure 8. Simulation results of the double sound source with the frequency 500 Hz.

5. Noise Source Localization and Identification Experiment

To verify the effectiveness and advantages of the proposed method in noise source localization and identification this section describes the noise source localization and identification experiments conducted for both single and double sound sources. In an open hall, an open SMA with 64 elements, randomly and uniformly distributed, was used to obtain the radiation signal of small speakers located at known positions. The experimental results were used to investigate the accuracy and effectiveness of the SMA extrapolation method in practical testing and the application effect of the proposed method in low-frequency noise source localization. The signal generator in the test transmission system generates a signal to drive the air sound source (small speaker) to radiate sound waves into the air. In the receiving system, the open SMA receives the signal, and then the B&K PULSE multi-channel data collector collects the data. Finally, the computer stores the data and displays the received signals of each element of the SMA in real time. The photos of the test site are shown in Figure 9. During the test, the two sound sources are located at $(1\,\mathrm{m}, 91°, 78°)$ and $(1\,\mathrm{m}, 89°, 160°)$ in the spherical coordinate system established with the center of the open SMA as the coordinate origin. In the single-source test, the transducer speaker located at $(1\,\mathrm{m}, 91°, 78°)$ was turned on. In the case of two sound sources test, the two speakers were turned on simultaneously.

(**a**) SMA and two loudspeakers (**b**) Data acquisition system and signal generators
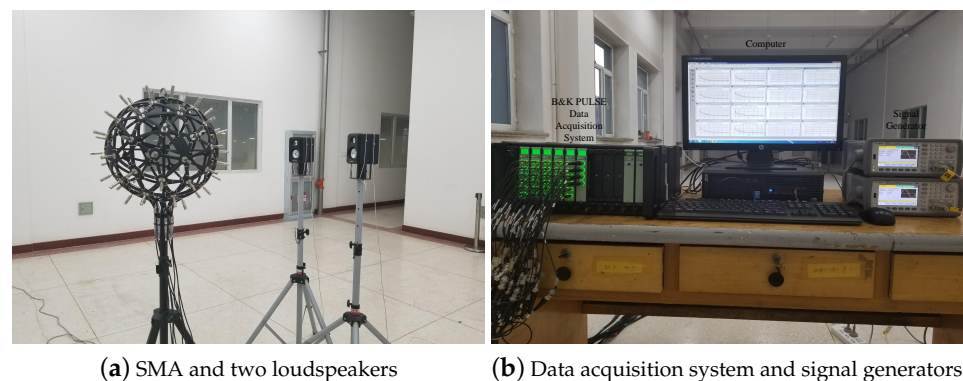
Figure 9. The set-up of the experiments conducted in a spacious room, with the SMA and the two loudspeakers tested shown in (**a**) and the B&K 64-channel PULSE Type 3660D data acquisition system and signal generators shown in (**b**).

5.1. Single Source Experiments

Figures 10 and 11 show the localization and identification results of the single noise source with the frequency 125 and 500 Hz, respectively. When comparing (a), (b) and (c) in Figures 10 and 11, it can be seen that the virtual SMA can effectively improve the localization effect. Moreover, it can be seen from (b) and (c) in Figures 10 and 11 that the GIB based on the joint processing of 'p+v' has a narrower main lobe and better localization effect than the other methods. However, due to the error of the difference processing, a little sidelobe interference appears in the proposed method shown in the result map, but it does not affect localization results.
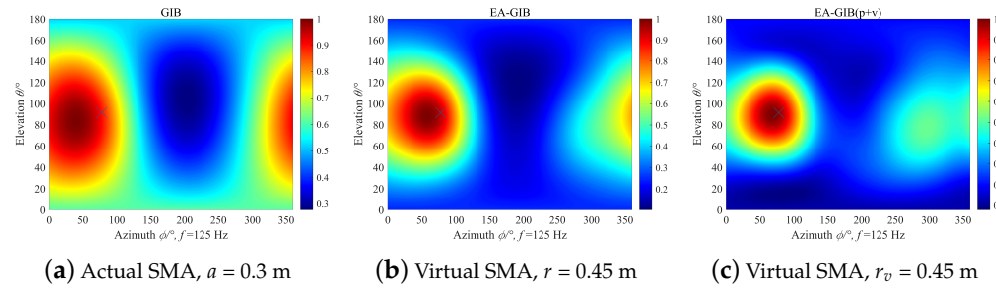
(**a**) Actual SMA, *a* = 0.3 m   (**b**) Virtual SMA, *r* = 0.45 m   (**c**) Virtual SMA, r_v = 0.45 m

Figure 10. Experiment data processing results of the single sound source with the frequency 125 Hz.

(**a**) Actual SMA, *a* = 0.3 m   (**b**) Virtual SMA, *r* = 0.45 m   (**c**) Virtual SMA, r_v = 0.45 m
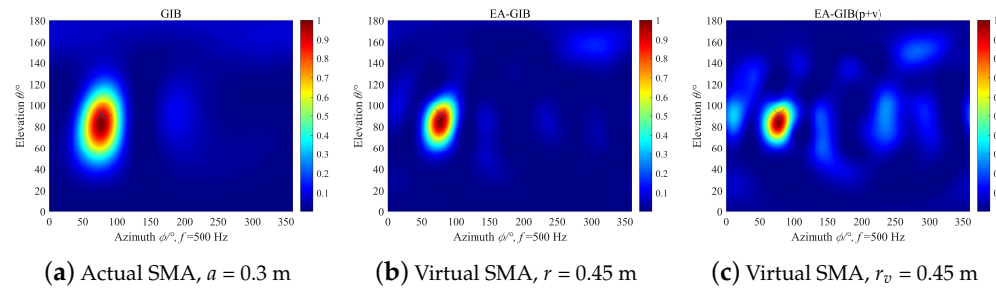
Figure 11. Experiment data processing results of the single sound source with the frequency 500 Hz.

5.2. Double Sources Experiments

Figures 12 and 13 show the localization and identification results of double noise source with the frequency is 250 and 500 Hz. When comparing (a), (b) and (c) in Figure 12, it can be seen that, in the sound source localization method, the direct used of the actual SMA cannot distinguish between two sound sources. After using the virtual SMA, the two sound sources can be effectively distinguished. In particular, the discrimination effect of the GIB using the 'p+v' joint processing proposed is more significant. As shown in Figure 13, with the increase in the sound source frequency, the actual SMA can distinguish between two sound sources, as can the GIB with the virtual SMA, but its advantages are not clear. In addition, experimental error, experimental environment and noise also affect the calculation result. Therefore, in actual applications, in order to ensure a good application effect, the radius of the virtual SMA should be reasonably selected by considering the SNR and extrapolation error.
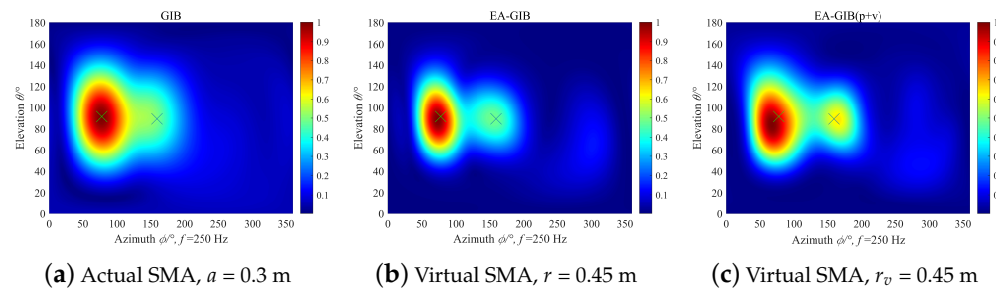

(**a**) Actual SMA, *a* = 0.3 m   (**b**) Virtual SMA, *r* = 0.45 m   (**c**) Virtual SMA, r_v = 0.45 m

Figure 12. Experiment data processing results of the double sound source with the frequency 250 Hz.

(**a**) Actual SMA, $a = 0.3$ m   (**b**) Virtual SMA, $r = 0.45$ m   (**c**) Virtual SMA, $r_v = 0.45$ m
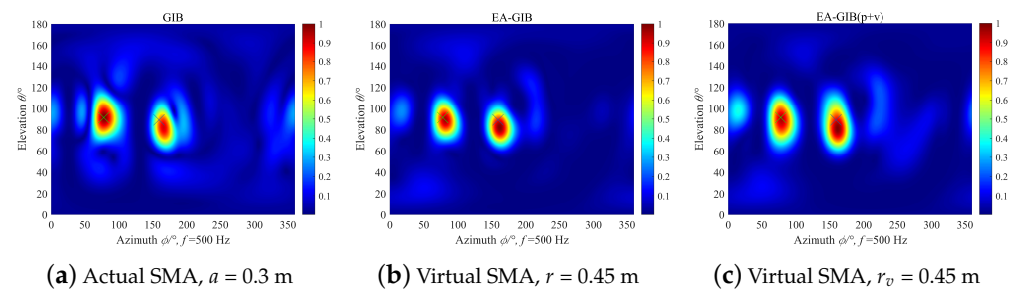
Figure 13. Experiment data processing results of the double sound source with the frequency 500 Hz.

6. Conclusions

With a focus on the spatial resolution problem of a small-aperture open SMA in low-frequency-noise-source localization, this paper proposes a high-resolution localization and identification method for low-frequency-noise-sources based on the joint processing of 'sound pressure and velocity' and the virtual dual-radius open SMA. Firstly, the virtual SMA with a larger aperture is obtained using the virtual SMA extrapolation method. Secondly, the virtual SMA and the actual SMA are used to obtain the approximate velocity by finite difference processing. At the same time, the virtual SMA extrapolation method is used to obtain the approximate sound pressure of the velocity position. Finally, using the velocity, approximate sound pressure, and the derived sound field transfer function of the 'p+v' joint processing mode, the vector signal processing technology is introduced into the GIB, which improves the low-frequency-noise-source localization and identification effect of the original actual SMA, broadening the application frequency range of the original SMA. The simulation and experiment results show that the extrapolation method, which can obtain a virtual larger-aperture SMA achieves a better spatial resolution than that of the actual SMA, and the GIB with the 'p+v' joint processing combining the extrapolation method has a better spatial resolution than the other methods and promising potential in engineering applications.

Author Contributions: Conceptualization, S.S. and B.Y.; methodology, S.S. and B.Y.; validation, B.Y.; formal analysis, S.S. and B.Y.; investigation, B.Y.; resources, S.S.; data curation, B.Y. and Q.G.; writing—original draft preparation, B.Y.; writing—review and editing, S.S. and Y.G.; supervision, S.S. All authors have read and agreed to the published version of the manuscript.

Institutional Review Board Statement: Not applicable.

Informed Consent Statement: Not applicable.

Data Availability Statement: Not applicable.

Conflicts of Interest: The authors declare no conflict of interest.

References

1. Haddad, K.; Hald, J. 3D localization of acoustic sources with a spherical array. *J. Acoust. Soc. Am.* **2008**, *123*, 3311. [CrossRef]
2. Sun, C.; Liu, Y. Spherical Reverse Beamforming for Sound Source Localization Based on the Inverse Method. *Sensors* **2019**, *19*, 2618. [CrossRef] [PubMed]
3. Chu, Z.; Yang, Y.; He, Y. Deconvolution for three-dimensional acoustic source identification based on spherical harmonics beamforming. *J. Sound Vib.* **2015**, *344*, 484–502. [CrossRef]
4. Meyer, J.; Elko, G. A highly scalable spherical microphone array based on an orthonormal decomposition of the soundfield. In Proceedings of the 2002 IEEE International Conference on Acoustics, Speech, and Signal Processing, Orlando, FL, USA, 13–17 May 2002; Volume 2, pp. II-1781–II-1784. [CrossRef]
5. Yang, B.; Shi, S.; Yang, D. Acoustic source localization using the open spherical microphone array in the low-frequency range. *MATEC Web Conf.* **2019**, *283*, 04001. [CrossRef]
6. Parthy, A.; Jin, C.; van Schaik, A. Measured and theoretical performance comparison of a co-centred rigid and open spherical microphone array. In Proceedings of the 2008 International Conference on Audio, Language and Image Processing, Shanghai, China, 7–9 July 2008; pp. 1289–1294. [CrossRef]

7. Hald, J. Spherical Beamforming with Enhanced Dynamic Range. *SAE Int. J. Passeng. Cars Mech. Syst.* **2013**, *6*, 1334–1341. [CrossRef]
8. Chu, Z.; Yang, Y. Comparison of deconvolution methods for the visualization of acoustic sources based on cross-spectral imaging function beamforming. *Mech. Syst. Signal Process.* **2014**, *48*, 404–422. [CrossRef]
9. Rafaely, B. Analysis and design of spherical microphone arrays. *IEEE Trans. Speech Audio Process.* **2005**, *13*, 135–143. [CrossRef]
10. Balmages, I.; Rafaely, B. Open-Sphere Designs for Spherical Microphone Arrays. *IEEE Trans. Audio Speech Lang. Process.* **2007**, *15*, 727–732. [CrossRef]
11. Rafaely, B.; Balmages, I.; Eger, L. High-resolution plane-wave decomposition in an auditorium using a dual-radius scanning spherical microphone array. *J. Acoust. Soc. Am.* **2007**, *122*, 2661–2668. [CrossRef] [PubMed]
12. Jin, C.T.; Epain, N.; Parthy, A. Design, Optimization and Evaluation of a Dual-Radius Spherical Microphone Array. *IEEE/ACM Trans. Audio Speech Lang. Process.* **2014**, *22*, 193–204. [CrossRef]
13. Zhang, Z.; Chen, S.; Xu, Z.; He, Y.; Li, S. Iterative regularization method in generalized inverse beamforming. *J. Sound Vib.* **2017**, *396*, 108–121. [CrossRef]
14. Gauthier, P.A.; Camier, C.; Pasco, Y.; Berry, A.; Chambatte, E.; Lapointe, R.; Delalay, M.A. Beamforming regularization matrix and inverse problems applied to sound field measurement and extrapolation using microphone array. *J. Sound Vib.* **2011**, *330*, 5852–5877. [CrossRef]
15. Padois, T.; Gauthier, P.A.; Berry, A. Inverse problem with beamforming regularization matrix applied to sound source localization in closed wind-tunnel using microphone array. *J. Sound Vib.* **2014**, *333*, 6858–6868. [CrossRef]
16. Li, M.; Lu, H.; Jin, J. Microphone distribution and spherical numerical integration for spherical nearfield acoustic holography. *Acta Acust.* **2015**, *40*, 695–702. [CrossRef]